



Relating atmospheric N₂O concentration to N₂O emission strength in the U. S. Corn Belt

Congsheng Fu^{1,2}, Xuhui Lee^{1,2}, Timothy J. Griffis³, Edward J. Dlugokencky⁴, Arlyn E. Andrews⁴

¹Yale-NUIST Center on Atmospheric Environment, Nanjing University of Information Science and Technology, Nanjing, Jiangsu, China

²School of Forestry and Environmental Studies, Yale University, New Haven, CT, USA

³Department of Soil, Water, and Climate, University of Minnesota, Saint Paul, MN, USA

⁴Global Monitoring Division, NOAA Earth System Research Laboratory, Boulder, Colorado, USA

Correspondence to: Xuhui Lee (xuhui.lee@yale.edu)

Abstract. Nitrous oxide (N₂O) has a high global warming potential and depletes stratospheric ozone. The U. S. Corn Belt plays an important role in the global anthropogenic N₂O budget. To date, studies on local surface N₂O emission and the atmospheric N₂O budget have commonly used Lagrangian models. In the present study, we used an Eulerian model - Weather Research and Forecasting Chemistry (WRF-Chem) model to investigate the relationships between N₂O emission in the Corn Belt and observed atmospheric N₂O mixing ratios. Modeled hourly N₂O mixing ratios were combined with continuous atmospheric N₂O measurements at the KCMP tall tower in Minnesota to constrain agricultural N₂O emissions. The modeled spatial patterns of atmospheric N₂O were validated against discrete observations at multiple tall towers in the NOAA flask network. After optimization of the surface flux, the model reproduced reasonably well the hourly N₂O mixing ratios monitored at the KCMP tower. Agricultural N₂O emissions in the EDGAR42 database needed to be scaled up by 19.0 to 28.1 fold to represent the true emission in the Corn Belt from June 1-20, 2010 - a peak emission period. Optimized total N₂O emissions were 3.00-4.38, 1.52-2.08, 0.61-0.81 and 0.56-0.75 nmol m⁻² s⁻¹ from June 1-20, August 1-20, October 1-20 and December 1-20, 2010, respectively. The simulated spatial patterns of atmospheric N₂O mixing ratios were in good agreement with the NOAA discrete observations during the strong emission peak in June. Such spatial patterns illustrate that the IPCC (Inter-governmental Panel on Climate Change) underestimate of emissions is not dependent on tower measurement location.

1 Introduction

Nitrous oxide (N₂O) is an important greenhouse gas whose global warming potential is 265 times that of CO₂ over a 100-year time horizon, and is the 3rd largest contributor to the increase in radiative forcing since 1750, only after CO₂ and CH₄ (Hofmann et al., 2006). In addition, N₂O has the largest ODP-weighted emissions of substances that deplete stratospheric ozone (Ravishankara et al., 2009). It is inert in the troposphere with a lifetime longer than one hundred years (Prather et al., 2012). Globally-averaged atmospheric N₂O has been increasing at a rate of 0.7 – 0.8 ppb yr⁻¹ since late-1970s (Prinn et al., 2000; Hall et al., 2007; Saikawa et al., 2014).

The U.S Corn Belt is an intensively managed agricultural region, where a substantial amount of nitrogen, approximately 7.7 Tg, is added to cropland in forms of synthetic fertilizer and manure each year (Griffis et al., 2013). The Corn Belt plays an important role in global anthropogenic N₂O emission (Miller et al., 2012). Cropland N₂O emission is difficult to measure due to the episodic nature of the emission and the high spatial variability (Wagner-Riddle et al., 2007; Groffman et al., 2009), and Corn Belt N₂O emission is no exception.

Bottom-up and top-down methods are used to quantify N₂O emissions from the Corn Belt and other agricultural regions (Corazza et al., 2011; Rees et al., 2013). The bottom-up method determines the total emission by multiplying N input or other



activity data with an emission factor for each pathway (De Klein et al., 2006). Top-down estimates of the emission are determined from observed atmospheric N₂O mixing ratios, a transport model and empirical equations for model optimization. Emissions inferred by the top-down method are generally larger than those by the bottom-up method for the Corn Belt. For example, Griffis et al. (2013) used three boundary layer budget methods and N₂O monitored on a tall tower in Minnesota during 5 2010 – 2011 to do a top-down analysis, and found that the N₂O emission in the Corn Belt was 3 to 9 times larger than bottom-up estimates, including estimates based on the IPCC inventory methodology and the EDGAR (Emission Database for Global Atmospheric Research) version 4.2 and GEIA (Global Emissions Initiative) databases. Kort et al. (2008) constrained the N₂O emission over the central U. S. and southern Canada using an inverse modeling method, and reported that emissions in EDGAR version 32FT200 and in GEIA are underestimated by about three fold for May – June, 2003. Similarly, the top-down analysis of 10 Miller et al. (2012) concluded that N₂O emissions in EDGAR4 (version 4.0) should be scaled by factors of 6.1 and 10.1 for June, 2004 and June, 2008, respectively, for the central U. S. Most recently, Chen et al. (2016) estimated N₂O emissions from the Corn Belt using a Bayesian inversion technique, concluding that both direct emissions from agricultural soils and indirect emissions from leaching and runoff are underestimated in EDGAR42, with the latter needing to be adjusted upward by 2.4 to 5.1 fold.

In the inverse analyses cited above, different emission databases (e.g., EDGAR 32 FT2000 and GEIA in Kort et al., 2008; 15 the Dynamic Land-Ecosystem Model – DLEM in Tian et al., 2010; EDGAR4, EDGAR 32 FT2000, GEIA, and DLEM in Miller et al., 2012 and Xiang et al., 2013; EDGAR42, GEIA, IPCC in Griffis et al., 2013; EDGAR42 and Community Land Model in Chen et al., 2016) are used to provide the *a priori* estimate of surface emissions, and the meteorological fields are simulated using mesoscale models such as the Weather Research and Forecasting (WRF) model (Skamarock et al., 2008) or regional reanalysis (Miller et al., 2012). The transport of N₂O in the atmosphere is usually simulated with the Stochastic Time Inverted 20 Lagrangian Transport (STILT) Model (Gerbig et al., 2003). An advantage of using STILT to conduct the inverse modeling for N₂O is that it needs much less computation resources than full three-dimensional Eulerian models.

Because Lagrangian models simulate the mixing ratio at one single point in space, they cannot quantify how the surface N₂O emissions influence the spatial characteristics of atmospheric N₂O mixing ratios. This problem is avoided by using Eulerian models. To the best of our knowledge, no modeling studies have been published on the relationship between the spatial 25 characteristics of surface emissions and the atmospheric N₂O mixing ratio at the regional scale. It is recognized that some of the parameterizations in STILT, such as the turbulent velocity variance and the Lagrangian timescale, need refinement to improve model performance (Pillai et al. 2012), and Eulerian modeling can inform these refinement efforts.

The WRF model coupled with chemistry (WRF-Chem) has been used to simulate the flux and transport of CO₂ (Ahmadov et al., 2009; Pillai et al., 2012) and CH₄ (Beck et al., 2013), and other reactive gases. We are not aware of WRF-Chem 30 applications to simulating the flux and transport of N₂O. In this study, we used WRF-Chem to investigate the spatial characteristics and influence of Corn Belt N₂O emissions on atmospheric N₂O. Specifically, we aimed to: (1) establish empirical relationships between the surface emission strength and the N₂O mixing ratio in the atmospheric boundary layer from multiple modeling experiments; (2) estimate the actual emission *via* a simple inverse analysis whereby these relationships were used to force agreement between modeled and observed atmospheric N₂O on a tall tower in Minnesota; and (3) investigate the spatial 35 patterns of the N₂O mixing ratio in the atmospheric boundary layer.

This work is complementary to a recent study completed by Chen et al. (2016). They used the Lagrangian-based STILT model to simulate N₂O transport, and conducted an inverse analysis using the Bayesian method. The present study used Eulerian-based WRF-Chem to model N₂O transport, and used a simple empirical equation to do the inverse analysis. The inverse analysis in Chen et al. (2016) was based on N₂O measured at a single height on a tower in Minnesota, while the present study used N₂O 40 measured at multiple heights on the same tower, and analyzed the influences of monitoring height on the inverse analysis results.



Additionally, the modeled N_2O mixing ratio in the present study was compared with observations of N_2O made by NOAA using discrete air samples collected at multiple sites.

2 Materials and methods

2.1 Observation

5 One set of atmospheric N_2O data came from observations at the KCMP radio communication tall tower (44.69°N , 93.07°W) in Minnesota, near the northern border of the Corn Belt (Fig. 1). Air was drawn from heights of 32, 56, 100, and 185 m above the ground into a tunable diode laser analyzer (TGA100A, Campbell Scientific Inc., Logan, Utah, USA) for continuous detection of the N_2O mixing ratio. Measurement was made at a sampling frequency of 10 Hz and was averaged to hourly values. The analyzer response was calibrated with standards on the NOAA 2006A N_2O mole fraction scale (Hall et al., 2007), and the hourly calibration precision was estimated to be 0.5 ppb. Details regarding the measurements of the N_2O mixing ratio were described in Griffis et al. (2010; 2013). Data of four periods at the KCMP tower were used in the present study, namely, 1st – 20th in June, August, October, and December in 2010, representing early summer, late summer, fall and winter, respectively. The month of June 2010 had particularly large emissions (Griffis et al., 2013).

15 The second dataset came from NOAA. Discrete air samples from six NOAA tall tower sites were collected daily during 18:00 – 21:00 (UTC) at heights of 107 – 457 m above the ground. The six sites are WBI (West Branch, Iowa), LEF (Park Falls, Wisconsin), SCT (Beech Island, South Carolina), BAO (Boulder Atmospheric Observatory, Colorado), AMT (Argyle, Maine), and WKT (Moody, Texas; Fig. 1). N_2O dry-air mole fractions were determined by gas chromatography with electron capture detection. The analytical system was calibrated with standards on the NOAA 2006A N_2O mole fraction scale. The average repeatability was ~0.4 ppb.

20 The third set of data is hourly N_2O mixing ratio monitored at Niwot Ridge (NWR), Colorado (40.04°N , 105.54°W ; elevation: 3018 m), which was used as background in the present study. The analyzer response was also calibrated with standards on the NOAA 2006A N_2O mole fraction scale. The reproducibility of N_2O calibrations in the ambient range was 0.22 ppb.

2.2 Model setup

25 The latest version of the WRF-Chem model (version 3.7.1) was used to simulate the meteorological field, and the transport and mixing of N_2O . In the model domain, N_2O was treated as a passive tracer. Fig. 1 shows the map of the Corn Belt, the locations of N_2O mixing ratio measurements, the modeling domains used in the present study, and the total default emission flux density according to EDGAR42 plus EDGAR2 natural soil emission. To represent the tall tower observations, atmospheric transport models should be configured with high spatial resolutions of 2 – 20 km (Phillai et al., 2012). In the modeling study of Miller et al. (2012), the outer and inner domains have a spatial resolution of 40 km and 10 km, respectively. In the present study, we deployed two nested domains. The outer domain had 44×189 grids with a resolution of 70 km, and the inner domain had 34×98 grids with a resolution of 10 km. Both domains had 40 vertical levels varying from the land surface to a pressure height of 50 hPa or approximately 20 km above the sea level.

35 Because three-dimensional modeling of the meteorological field and the tracer transport requires substantial computational resources, it is not feasible to do the simulation continuously for a long period (e.g., one year). Instead, the model calculation was performed for four select periods (1st – 20th in June, August, October, and December in 2010). The initial and boundary conditions for the meteorological field were obtained from the weather forecast model Global Forecast System



(ftp://nomads.ncdc.noaa.gov/GFS/analysis_only). The initial and boundary conditions for the N₂O mixing ratio for each modeling period were obtained from Model for Ozone and Related Chemical Tracers (MOZART) version 4 (http://www.acom.ucar.edu/wrf-chem/mozart.shtml). Cloud microphysics was represented with the single-moment 5-class scheme (WSM), the boundary layer was modeled with the Yonsei University Scheme (YSU), and the land surface was modeled with the Community Land Model Version 4 (CLM4). Other model settings are shown in Table 1.

The lower boundary condition for N₂O was a predetermined surface emission flux, which was constant in time but varied spatially. Both the EDGAR and the GEIA databases have surface emission data for the Corn Belt, and both have more detailed spatial distributions than DLEM (Miller et al., 2012). Because EDGAR needs less magnitude correction than GEIA in inverse modeling (Miller et al., 2012; Griffis et al., 2013), we used the latest version of EDGAR (version 4.2) as the default flux boundary condition. EDGAR42 N₂O emission data has a spatial resolution of 0.1° × 0.1°, close to the resolution of our inner model domain. The total EDGAR42 N₂O emission (annual mean flux density) for the outer domain is 0.083 nmol m⁻² s⁻¹, and corresponding value for the Corn Belt is 0.21 nmol m⁻² s⁻¹. Agricultural sources of N₂O include manure management, agricultural soil, indirect emission from agriculture, and agricultural biomass burning. The total agricultural emission rate is 0.15 nmol m⁻² s⁻¹ for the Corn Belt. The natural soil emission rates are 0.036 and 0.038 nmol m⁻² s⁻¹ for the outer domain and the Corn Belt, respectively. The spatial distribution of the sum of the EDGAR42 flux and natural soil emission is shown in Fig. 1.

2.3 Experimental design

Because N₂O is inert in the troposphere, changes in its mixing ratio C are primarily controlled by variations in the surface source strength F . However, the relationship between C and F is not a 1:1 correspondence. Because of influences of wind direction and vertical diffusion, we do not expect the C enhancement in the atmospheric boundary layer to double in response to a doubling of F in the Corn Belt. Here we established the relationship between C and F using results of multiple model runs. Three different modeling experiments were conducted for each of the four study periods. The first run was a background simulation using the natural soil emission and EDGAR42 non-agricultural emissions for both domains. The resulting N₂O mixing ratio is taken as the background, C_b . The second model run was a default simulation driven by natural soil emission and the total EDGAR42 emission (agricultural and non-agricultural) in both domains. The third run was a scaled simulation whereby the surface flux in the grid cells in the inner domain was the sum of natural soil emission, EDGAR42 non-agricultural emissions, and a multiple of EDGAR42 agricultural emissions. The multiplier values are 3, 6, 12, and 25, the exact choice depending on the modeling period (Table 2).

We define the concentration enhancement, ΔC , for the grid cell containing KCMP tower as the difference in N₂O mole fraction between the default or scaled simulation and the background simulation. Let concentration multiplier M_C be the ratio of ΔC from the scaled simulation to that from the default simulation and M_F be the emission flux multiplier. The two multipliers are related to one another as

$$M_C - 1 = a (M_F - 1) \quad (1)$$

where the empirical coefficient a (< 1) was determined with a least squares procedure from the modeled concentration data.

2.4 A simple inverse analysis

We used the observed enhancement, ΔC , defined as the actual concentration observed at the KCMP tall tower minus a background concentration, to constrain the surface emission flux. The background concentration was observed at NWR, which is upwind of and outside the Corn Belt. The background value was calculated as a 3-day running mean.



If the EDGAR42 emission flux is accurate and the model is perfect, the observed ΔC should match with the concentration enhancement from the default model simulation. Any disagreement is caused either by model errors or by errors in the surface flux. Here we assume that the flux errors are solely responsible for the disagreement, leaving the discussion of model errors to a later part of the paper. Not surprisingly, the ΔC from the default simulation is always lower than the observed ΔC , meaning that the EDGAR42 emission flux is biased low. To find a correction factor, we should ideally run the WRF-Chem in an iterative fashion, by adjusting the surface flux repeatedly until the modeled ΔC matches the observed ΔC . However, this procedure is computationally prohibitive. Instead, we resorted to a simple two-step method. First, the concentration multiplier M_C was determined by dividing the mean observed ΔC with the mean modeled ΔC from the default simulation for each modeling period. Second, the M_C value was used in Equation 1 to find the emission multiplier M_F . The EDGAR42 agricultural emission flux times M_F is then regarded as the true agricultural flux.

An implicit assumption in this simple inverse analysis is that ΔC should respond linearly to changes in the surface flux. Because N_2O is an inert gas, this assumption is generally satisfied (see Fig. 2 below).

3 Results

3.1 Emission enhancement versus concentration enhancement at the KCMP site

Because the KCMP tower is close to the northern boundary of the Corn Belt (Fig. 1), south wind is expected to cause larger N_2O mixing ratio enhancement than north wind. In Fig. 2a-c, the modeled ΔC at the height of 185 m from the scaled simulation with a flux multiplier M_F of 25 is plotted against the modeled ΔC from the default simulation for the time period from June 1 to 20, 2010. Each data point represents one hourly value. The data are sorted into three wind direction groups ($90^\circ - 270^\circ$, $270^\circ - 90^\circ$, and $0^\circ - 360^\circ$). Of the three wind groups, south wind with direction of $90^\circ - 270^\circ$ resulted in the largest N_2O mixing ratio enhancement (Fig. 2b). The regression slope for this wind direction range is 18.66. In other words, at the flux multiplier M_F of 25, the concentration enhancement multiplier M_C is 18.66. The concentration multiplier is 11.47 for north wind (wind direction range $270^\circ - 90^\circ$; Fig 2c) and is 15.71 if all wind directions are considered (Fig. 2a).

Similar analysis was applied to the other three modeling periods, each yielding a M_C value for each wind sector at the set M_F value given in Table 2. When the M_C versus M_F data pairs are put together for all four periods, a clear linear relationship is evident (Fig. 2d-f). Equation 1 with a coefficient value a of 0.740 best describes this relationship for south winds according to the least squares regression. The coefficient value is 0.470 for north winds and 0.631 for all wind directions. The value a of 0.740 for south winds is used for the inverse analysis presented below.

3.2 Constrained agricultural emission

Because the KCMP site is close to the northern boundary of the Corn Belt, the observed N_2O mixing ratio could reasonably reflect emissions from the Corn Belt only during southerly winds. Therefore, data obtained for southerly flow were used to constrain the surface emission. As explained in Section 2.4, the concentration multiplier M_C was computed as the ratio of the mean ΔC observed in south wind at the 185 m height to the mean ΔC from the default model simulation at the same height and also in south wind conditions. This M_C value was then used in Equation 1 with $a = 0.740$ to find the flux multiplier M_F . For example, for June 1-20, the concentration multiplier is 21.0, and the optimized flux multiplier is 28.1.



Table 2 shows the constrained N_2O emission from the Corn Belt using the N_2O mixing ratio monitored at the height of 185 m on the KCMP tower. The constrained agricultural N_2O emissions for the 1st – 20th in June, August, October, and December are 4.29, 1.99, 0.72, and 0.66 $\text{nmol m}^{-2} \text{s}^{-1}$, respectively.

3.3 Comparison of observed and adjusted model N_2O concentration

5 Fig. 3 shows the observed (grey line), modeled (red line), and the adjusted model (blue line) N_2O mixing ratio enhancement at 185 m on the KCMP tower. The modeled ΔC here is the concentration difference between the default simulation and the background simulation, and the adjusted model ΔC is the default ΔC times the appropriate concentration multiplier. The modeled ΔC using the default emission is clearly smaller than observation for all four periods (Fig. 3). For example, for the model period June 1-20, the default model ΔC value is 0.18 and 0.19 ppb for all wind directions and for south wind, respectively,
10 whereas the observed mean ΔC is 4.95 and 5.44 ppb, respectively. The south wind results yield a concentration multiplier of 28.1. After the adjustment, the modeled mixing ratio enhancements are much closer to the observations than those from the default simulation. The adjusted model ΔC can roughly reproduce the temporal fluctuations of the observed ΔC at the KCMP site, although the substantial noises (abrupt increases and decreases) in the observation result in low correlation coefficients between the simulated and the observed time series.

15 As shown in Fig. 2a-c, wind direction clearly affects the simulated ΔC . For the four study periods, the mean simulated ΔC under north wind conditions was roughly half of that under south wind conditions. The wind direction influence is also evident in the hourly time variations of ΔC . For example, southern wind (wind direction $90^\circ - 270^\circ$) prevailed during the four-day period from day of year 280 to 284, and the mixing ratio showed a gradual increasing trend with time.

20 Another factor that drives the temporal fluctuations of ΔC is the diurnal change of vertical mixing which is stronger in the day than at night. The larger daytime vertical diffusivity corresponds to the smaller modeled N_2O mixing ratio enhancement near the land surface. The intensity of vertical mixing can be reflected by the mixed layer height. The linear correlation coefficient between the modeled mixed layer height and the hourly modeled ΔC was -0.45 and -0.19 for the KCMP grid at heights of 32 m and 185 m in August, respectively. The corresponding correlation values were -0.53 and -0.35 in October, -0.35 and -0.12 in June, and -0.32, and -0.15 in December. All of these correlations are significant (confidence level $p < 0.01$).

25 Accurate assessment of the model performance is difficult at hourly intervals because of large measurement noises. Here we compare the observed daily mean values with the daily simulated mean values using the default emission, and the adjusted results (Fig. 4). Without the flux adjustments, the modeled daily mean ΔC is an order of magnitude smaller than the observed value. After the adjustments, the model result is closer to the observation, with a linear regression slope of 0.76, and R^2 also improved from 0.01 before the adjustments to 0.31. Here one single concentration multiplier M_C value obtained for south wind
30 conditions (e.g., $M_C = 21.0$ for June 1 - 20) was used to make the concentration adjustment to all hourly model values for each period, regardless of actual wind direction, and the daily mean adjusted value was based on these hourly adjusted values. If the adjustments are made separately to southern winds and to northern winds using the two different regression equations (Figure 2e and 2f), the adjusted daily model mean ΔC is improved even further: the regression slope of the adjusted model ΔC against the observed ΔC is 0.94 and the R^2 is 0.34.

35 3.4 Spatial variations of modeled N_2O concentration

Fig. 5a illustrates the mean modeled ΔC during June 1 – 20 for the modeling area from the scaled simulation run with a flux multiplier of 25.0, and Fig. 5b shows similar results as Fig. 5a but only for UTC hours 19 and 20. In Fig. 5a, the maximum mean



enhancement is 5.92 ppb, found at 93.20°W and 42.12° N, which is near the center of the Corn Belt and 286 km south of the KCMP tower. The mean modeled ΔC for the whole Corn Belt is 4.15 ppb at the height of 185 m above the ground, illustrating a clear influence of the Corn Belt on atmospheric N_2O .

The mean modeled ΔC at the KCMP tower is 3.69 ppb, slightly lower than the observed value of 4.95 ppb. Two reasons explain this low bias. First, the results shown in Fig. 5 were from the scaled simulation with an experimental flux multiplier of 25.0, and this multiplier is smaller than the optimized flux multiplier M_F value of 28.1 determined in post-simulation analysis. Second, the flux multiplier was calibrated to match the modeled results to observations during southerly winds, instead of all-wind conditions.

The modeled ΔC distribution resembles a rectangle that surrounds the Corn Belt, with a narrow dimension in the south-north direction and a wide dimension in the east-west direction, implying a larger spatial gradient in the south-north direction than in the east-west direction.

4 Discussion

4.1 Model accuracy

A key factor in inverse analysis is modeling accuracy. One source of model error stems from the vertical diffusion calculation. Previous studies have shown that the scheme describing diffusion in WRF-Chem affects modeled scalar concentrations in the atmospheric boundary layer (Kretschmer et al., 2012). If diffusion is too strong, the emitted N_2O will spread over a deeper boundary layer, potentially causing a low bias in the modeled ΔC near the surface. The YSU diffusion scheme adopted in this study has been used successfully in previous WRF simulations (e.g., Pillai et al., 2012). Accuracy assessment results from Pillai et al. (2012) indicate that WRF-Chem using the YSU scheme can capture the hourly fluctuations of passive tracers at different heights near the ground.

The sensitivity to the diffusion scheme is manifested in the predicted mixed layer height z_i because a high bias in z_i will lead to a low bias in ΔC and vice versa. In an inverse modeling analysis of carbon monoxide, Kim et al. (2013) presented the diurnal cycle of z_i from four different meteorological simulations for the KCMP tower site, namely, EDAS (Eta Data Assimilation System), NARR (North American Regional Reanalysis) from the National Centers for Environmental Prediction (NCEP), BRAMS (Brazilian developments on the Regional Atmospheric Modeling System), and GEOS-5 (Goddard Earth Observing System Model, version 5). Their inverse analysis yields surface carbon monoxide emission estimates with reasonable accuracy, achieving an R value of 0.69 between the measured and simulated CO mixing ratios. Fig. 6 compares our modeled z_i diurnal cycle with those derived for 2009 from the three meteorological simulations (EDAS, NARR, and GEOS-5) in Kim et al. (2013) and with the 3-hourly NCEP-NARR data for the four exact 20-day periods in 2010. In this comparison we omitted the BRAMS data because its z_i value is unreasonably high (Kim et al., 2013). Our modeled mean diurnal cycles of the mixing height during 1st – 20th in June, August, and October are broadly consistent with the results of NARR and with those reported by Kim et al. (2013). Even though the results in Kim et al. (2013) are for complete seasons in 2009 and the results in the present study are for shorter periods in 2010, this is a valid comparison because our summer periods occurred at the beginning and the end of the season and our fall period was in the middle of the season. For December 1st – 20th, our z_i value is biased high by ~ 400 m and shows smaller diurnal variations in comparison with NARR. For this reason, we are less confident about the inverse result for this time period than for the other three time periods.

We also assessed model accuracy by comparing the simulated ΔC with measurements of N_2O in discrete samples collected at sites in NOAA's tall tower network (Fig. 5b and Table 3). In this comparison, the modeled ΔC value is the average of UTC



hours 19 and 20 and interpolated to the measurement height of each site. Fig.5b was produced from the model simulation with an experimental flux multiplier of 25.0 which is reasonably close to the optimized flux multiplier of 28.1. In Table 3, two model values are given, one from the default simulation with the experimental $M_F = 1$ and the other from the simulation whose M_F is closest to the optimized M_F for the given period. The modeled ΔC with $M_F = 25.0$ agrees reasonably well with the observations at WBI, LEF, SCT, and BAO for June 1st – 20th. Both the observed and modeled ΔC are largest at WBI, which is close to the center of the Corn Belt, among the six NOAA-PFP sites. The next highest ΔC is found at LEF, although a high model bias is evident there. The modeled and observed mean ΔC of these four sites located in the model domain are 1.51 and 1.27 ppb, respectively.

For August, October, and December with much weaker emissions than in June, the agreement between the observed and modeled ΔC is not as good. The observed N_2O mixing ratio at WBI near the center of the Corn Belt is even smaller than that at the background during October 1-20, as indicated by the negative ΔC (Table 3), which seems unreasonable. Large variations in the concentration measurements are a potential cause of this problem. For example, the standard deviation of the measurement at WBI is 0.76 ppb for October 1 – 20, 2010, which is larger than the concentration enhancement we tried to model. Furthermore, the number of samples (27 points per period on average) is not large enough to reduce the standard error or variability of the measurement mean value. The largest disagreement occurred in the October period: the modeled mean ΔC with $M_F = 3.0$ is 0.81 ppb for the four sites in the model domain but the observed mean ΔC is actually 0.01 ppb.

By measuring spatial variations in atmospheric N_2O , an observational network consisting of multiple sites has the potential to help constrain inverse analysis using Eulerian tracer transport models. Given the flask measurement variability, such N_2O inversion would be difficult for low emission periods. The large measurement variability may have explained why Miller et al. (2012) limited their geostatistical inversion to an early summer period. In this regard, the continuous observations at KCMP and NWR are more appropriate for inverse analysis because they produce more robust mean values than the flask observations.

4.2 Sensitivity to measurement height

The analysis presented above is based on observations from 185 m on the KCMP tower. The inverse analysis was also repeated with observations from the heights of 32 m and 100 m. The optimized flux multipliers are summarized in Table 2. It is interesting that the optimized flux multiplier or the constrained emission flux increases with the observational height. The constrained flux is lowest if KCMP data obtained at 32 m were used and largest for data at 185 m. Theoretically, the constrained emission should be independent of mixing ratio observation height if the N_2O mixing ratio is perfectly simulated. To help explain the height dependence, we compared the observed and modeled vertical N_2O mixing ratio gradients between 32 m and 185 m. Both observed and modeled gradients were close to zero during the majority of the daytime periods (11:00 - 18:00 local time), with the mean value of (concentration at 32 m minus that at 185 m) 0.03 (observation) and 0.25 ppb (model) during 11:00 - 18:00 for June 1-20, illustrating strong vertical mixing in daylight hours. Here the model result was based on the simulation with an experimental flux multiplier of 25.0. During this period, the nighttime (21:00 - 06:00) gradient is greater, with the mean value of 1.44 ppb according to the observation and 5.47 ppb according to the model simulation. A similar diurnal pattern of the N_2O concentration gradient is also reported by Zhang et al. (2014). In the present study, the difference in vertical gradient between simulation and observation during night (5.47 ppb versus 1.44 ppb) is much larger than that during daytime (0.25 ppb versus 0.03 ppb), and contributes the most to the height dependence of the constrained emission flux.

We suggest that the bias in the modeled mixing ratio gradient and the height dependence of the constrained emission flux are mainly consequences of different footprints between the monitoring heights. According to STILT modeling results, the footprint for the height of 100 m at KCMP covers most of the continental U. S., and that for 185 m is at the continental scale (Kim et al., 2013; Chen et al., 2016), both of which are larger than the Corn Belt itself. As shown by Kort et al. (2008) and Miller



et al. (2012), emissions outside the Corn Belt are probably underestimated by EDGAR database too. In other words, the concentration enhancement observed at 100 and 185 m at KCMP had contributions from agricultural sources both within and outside the Corn Belt, although being closer to the observation tower, the latter should outweigh the former. But in our analysis, adjustment was made only to the sources within the Corn Belt. To compensate for the EDGAR bias outside the belt, a large flux multiplier is required to force agreement between the modeled concentration and the observation at 100 or 185 m. Evidently, at nighttime when vertical mixing is weak, this large flux adjustment causes the modeled concentration at 32 m to increase more than that at 185 m, resulting in a high bias in the modeled concentration gradient. In this regard, the emission flux constrained with the data obtained at 32 m reflects more local sources than those constrained with the data obtained at higher levels, and may be a more accurate estimate of the emissions in the Corn Belt, considering that the landscapes around the KCMP tower are representative of the entire Corn Belt (Griffis et al., 2013).

4.3 Comparison with other emissions estimates

According to our inverse analysis, agricultural N_2O emissions in the Corn Belt are 19.0 to 28.1 times the default EDGAR42 agricultural emissions during June 1 – 20, 2010, corresponding to an actual emission flux density of $2.91 - 4.29 \text{ nmol m}^{-2} \text{ s}^{-1}$, with the upper and lower bounds determined by the concentration observed at 185 and 32 m, respectively. The total emission, including agricultural, natural soil and non-agricultural sources is $3.00 - 4.38 \text{ nmol m}^{-2} \text{ s}^{-1}$. Using a nocturnal boundary layer method, Griffis et al. (2013) estimated that the Corn Belt emission flux is $\sim 2.0 - 2.5 \text{ nmol m}^{-2} \text{ s}^{-1}$ in June and July 2010, which is $\sim 0.5 - 1.0 \text{ nmol m}^{-2} \text{ s}^{-1}$ smaller than the lower bound of this study. From the results presented in Kort et al. (2008), we infer that their constrained N_2O emission is about $0.56 \text{ nmol m}^{-2} \text{ s}^{-1}$ in May – June, 2003 for the Corn Belt. Miller et al. (2012) reported that maximum emissions occurred in June in both 2004 and 2008, and their constrained emission in June, 2008 is approximately $1.20 \text{ nmol m}^{-2} \text{ s}^{-1}$ for the Corn Belt.

The differences between the present study and the previous studies are partly caused by the different spatial scales involved. In both the studies by Kort et al. (2008) and Miller et al. (2012), a single emission scaling is applied to the entire modeling region (the continental U. S. and southern Canada in Kort et al., 2008; the central U. S. in Miller et al., 2012), instead of scaling the emission for the Corn Belt only as in the present study. If they scaled the emissions for the Corn Belt only, the resulting emission flux would have been larger.

Different study duration, time of the year, and study year also contribute to the different constrained emissions between the present and the former studies. In the present study, the early summer study period (June 1-20, 2010) is short and is timed with highest emission events. If we average the early summer and late summer (August 1 – 20), the emission flux is reduced to $2.26 - 3.23 \text{ nmol m}^{-2} \text{ s}^{-1}$. Additionally, Kort et al. (2008) studied 2003 and Miller et al. (2012) studied 2008. The differences in the emission flux can be a result of increasing emission with time. Based on our ongoing study, the N fertilizer input to the Corn Belt has averaged $6.2 \pm 0.9 \text{ Tg N}$ per year, and the trend is about 0.08 Tg N per year increase.

Our simulation results illustrate that the emission strength decreases quickly after August (Table 3; Fig. 3), and such seasonal changes in 2010 in the present study are consistent with the results for other years in former inverse studies. For example, a quick decrease of N_2O emission strength since August also occurred in 2008 (Miller et al., 2012) and in 2009 (Zhang et al., 2014).

Our study confirms that the emission database EDGAR42 significantly underestimates agricultural N_2O emission in the Corn Belt. Although our simple inverse analysis cannot identify which agricultural emission categories suffer biases, two recent studies indicate that the underestimation occurs to the indirect emission associated with runoff and leaching. Turner et al. (2015) measured N_2O emissions from headwater streams in the Corn Belt, and reported that the IPCC indirect emission factors for rivers



are underestimated up to nine fold in southern Minnesota. Using the STILT model and a Bayesian inversion technique, Chen et al. (2016) reported that the indirect emission flux in the Corn Belt is 2.4 – 5.1 fold as large as that estimated by the IPCC inventory methodology. Complementary to former Lagrangian approaches, the Eulerian approach used here places a spatially explicit constraint on the underestimate problem, illustrating that the IPCC underestimate is not dependent on tower measurement location, i.e. WBI and KCMP would yield similar conclusions.

5 Summary

In the present study, we investigated the relationships between the N₂O emission from the Corn Belt and the atmospheric N₂O mixing ratio using the WRF-Chem model, derived simple empirical equations for relating changes in the atmospheric mixing ratio to changes in the surface emission flux, and used the hourly N₂O mixing ratio monitored at the KCMP tower to constrain the agricultural N₂O emission. The key findings are summarized as follows:

- By treating N₂O as an inert tracer, the WRF-Chem model could simulate atmospheric N₂O at high temporal (hourly) and spatial (10 km) resolutions and with reasonable accuracy. Following surface flux optimization, the model explain 31% (185 m) – 35% (32 m) of the observed variations in the daily mean N₂O mixing ratio at KCMP.
- The EDGAR42 database underestimated agricultural N₂O emissions in the Corn Belt for all four model periods (1st to 20th in June, August, October and December, 2010). The largest bias occurred in June: a simple inverse analysis indicates that actual agricultural emissions were 19.0 to 28.1 times EDGAR42 emissions.
- According to our inverse analysis, the total emission, including natural soil emissions and total EDGAR42 emissions (agricultural and non-agricultural), was 3.00-4.38, 1.52-2.08, 0.61-0.81 and 0.56-0.75 nmol m⁻² s⁻¹ in June, August, October and December 2010, respectively. The lower and upper bounds of these ranges were determined with observations at 32 m and 185 m on the KCMP tower, respectively.
- The simulated spatial patterns of atmospheric N₂O mixing ratios are in good agreement with observations from discrete air samples made by the NOAA during June, which is a strong emission peak. In the other three modeling periods, the modeled mixing ratio and the network observations show some disparity. The IPCC underestimate of agricultural N₂O emissions in the Corn Belt is not dependent on tower measurement location.

Acknowledgements. This study was funded by a grant supported by the United States Department of Agriculture grant USDA-NIFA 2013-67019-21364. This research used resources of the National Energy Research Scientific Computing Center, a DOE Office of Science User Facility supported by the Office of Science of the U.S. Department of Energy under Contract No. DE-AC02-05CH11231.

References

- Ahmadov, R., Gerbig, C., Kretschmer, R., Körner, S., Rödenbeck, C., Bousquet, P., and Ramonet, M.: Comparing high resolution WRF-VPRM simulations and two global CO₂ transport models with coastal tower measurements of CO₂, Biogeosciences, 6, 807-817, doi:10.5194/bg-6-807-2009, 2009.
- Beck, V., Gerbig, C., Koch, T., Bela, M. M., Longo, K. M., Freitas, S. R., Kaplan, J. O., Prigent, C., Bergamaschi, P., and



- Heimann, M.: WRF-Chem simulations in the Amazon region during wet and dry season transitions: evaluation of methane models and wetland inundation maps, *Atmos. Chem. Phys.*, 13, 7961-7982, doi:10.5194/acp-13-7961-2013, 2013.
- Corazza, M., Bergamaschi, P., Vermeulen, A. T., Aalto, T., Haszpra, L., Meinhardt, F., O'Doherty, S., Thompson, R., Moncrieff, J., Popa, E., Steinbacher, M., Jordan, A., Dlugokencky, E., Brühl, C., Krol, M., and Dentener, F.: Inverse modelling of European N₂O emissions: assimilating observations from different networks, *Atmos. Chem. Phys.*, 11, 2381-2398, doi:10.5194/acp-11-2381-2011, 2011.
- Chen, Z., Griffis, T. J., Millet, D. B., Wood, J., Lee, X., Baker, J. M., Xiao, K., Turner, P., Chen, M., and Zobitz, J.: Partitioning N₂O emissions within the US Corn Belt using an inverse modeling approach, 2016. *Global Biogeochemical Cycles*, in press.
- De Klein, C., Novoa, R. S. A., Ogle, S., Smith, K. A., Rochette, P., Wirth, T. C., McConkey, B. G., Mosier, A., and Rypdal, K.: N₂O emissions from managed soils, and CO₂ emissions from lime and urea application, in 2006 IPCC Guidelines for National Greenhouse Gas Inventories, Vol 4: Agriculture, Forestry and Other Land Use, edited by H. S. Eggleston et al., pp. 11.11–11.54, Institute for Global Environmental Strategies (IGES), Intergovernmental Panel on Climate Change (IPCC), Kanagawa, Japan, 2006.
- Gerbig, C., Lin, J. C., Wofsy, S. C., Daube, B. C., Andrews, A. E., Stephens, B. B., Bakwin, P. S., and Grainger, C. A.: Toward constraining regional-scale fluxes of CO₂ with atmospheric observations over a continent: 2. Analysis of COBRA data using a receptor-oriented framework, *J. Geophys. Res.-Atmos.*, 108, 4757, doi:10.1029/2003JD003770, 2003.
- Griffis, T. J., Baker, J. M., Sargent, S. D., Erickson, M., Corcoran, J., Chen, M., and Billmark, K.: Influence of C₄ vegetation on ¹³CO₂ discrimination and isoforcing in the upper Midwest, United States, *Global Biogeochem. Cycles*, 24, GB4006, doi:10.1029/2009GB003768, 2010.
- Griffis, T. J., Lee, X., Baker, J. M., Russelle, M. P., Zhang, X., Venterea, R., and Millet, D. B.: Reconciling the differences between top-down and bottom-up estimates of nitrous oxide emissions for the U.S. Corn Belt, *Global Biogeochem. Cycles*, 27, 746–754, doi:10.1002/gbc.20066, 2013.
- Groffman, P. M., Butterbach-Bahl, K., Fulweiler, R. W., Gold, A. J., Morse, J. L., Stander, E. K., Tague, C., Tonitto, C., and Vidon, P.: Challenges to incorporating spatially and temporally explicit phenomena (hotspots and hot moments) in denitrification models, *Biogeochemistry*, 93(1-2), 49–77, doi: 10.1007/s10533-008-9277-5, 2009.
- Hall, B. D., Dutton, G. S., and Elkins, J. W.: The NOAA nitrous oxide standard scale for atmospheric observations, *J. Geophys. Res.*, 112, D09305, doi:10.1029/2006JD007954, 2007.
- Hofmann, D. J., Butler, J. H., Dlugokencky, E. J., Elkins, J. W., Masarie, K., Montzka, S. A., and Tans, P.: The role of carbon dioxide in climate forcing from 1979 – 2004: Introduction of the annual greenhouse gas index, *Tellus, Ser. B*, 58, 614–619, doi: 10.1111/j.1600-0889.2006.00201.x, 2006.
- Kim, S. Y., Millet, D. B., Hu, L., Mohr, M. J., Griffis, T. J., Wen, D., Lin, J. C., Miller, S. M., and Longo, M.: Constraints on Carbon Monoxide Emissions Based on Tall Tower Measurements in the U.S. Upper Midwest, *Environ. Sci. Technol.*, 47(15), 8316–8324, do: 10.1021/es4009486, 2013.
- Kort, E. A., Eluszkiewicz, J., Stephens, B. B., Miller, J. B., Gerbig, C., Nehr Korn, T., Daube, B. C., Kaplan, J. O., Houweling, S., and Wofsy, S. C.: Emissions of CH₄ and N₂O over the United States and Canada based on a receptor-oriented modeling framework and COBRA-NA atmospheric observations, *Geophys. Res. Lett.*, 35, L18808, doi:10.1029/2008GL034031, 2008.
- Kretschmer, R., Gerbig, C., Karstens, U., and Koch, F.-T.: Error characterization of CO₂ vertical mixing in the atmospheric transport model WRF-VPRM, *Atmos. Chem. Phys.*, 12, 2441-2458, doi:10.5194/acp-12-2441-2012, 2012.
- Miller, S. M., Kort, E. A., Hirsch, A. I., Dlugokencky, E. J., Andrews, A. E., Xu, X., Tian, H., Nehr Korn, T., Eluszkiewicz, J.,



- Michalak, A. M., and Wofsy, S. C.: Regional sources of nitrous oxide over the United States: Seasonal variation and spatial distribution, *J. Geophys. Res.*, 117, D06310, doi:10.1029/2011JD016951, 2012.
- Pielke, R. A., Cotton, W. R., Walko, R. L., Tremback, C. J., Lyons, W. A., Grasso, L. D., Nicholls, M. E., Moran, M. D., Wesley, D. A., Lee, T. J., Copeland, J. H.: A comprehensive meteorological modeling system—RAMS, *Meteorol. Atmos. Phys.*, 49(1–4), 69–91, 1992.
- Pillai, D., Gerbig, C., Kretschmer, R., Beck, V., Karstens, U., Neining, B., and Heimann, M.: Comparing Lagrangian and Eulerian models for CO₂ transport – a step towards Bayesian inverse modeling using WRF/STILT-VPRM, *Atmos. Chem. Phys.*, 12, 8979–8991, doi:10.5194/acp-12-8979-2012, 2012.
- Prather, M. J., Holmes, C. D., and Hsu, J.: Reactive greenhouse gas scenarios: Systematic exploration of uncertainties and the role of atmospheric chemistry, *Geophys. Res. Lett.*, 39, L09803, doi:10.1029/2012GL051440, 2012.
- Prinn, R. G., Weiss, R. F., Fraser, P. J., Simmonds, P. G., Cunnold, D. M., Alyea, F. N., O'Doherty, S., Salameh, P., Miller, B. R., Huang, J., Wang, R. H. J., Hartley, D. E., Harth, C., Steele, L. P., Sturrock, G., Midgley, P. M., McCulloch, A.: A history of chemically and radiatively important gases in air deduced from ALE/GAGE/AGAGE, *J. Geophys. Res.*, 105, 17,751–17,792, doi: 10.1029/2000JD900141, 2000.
- Ravishankara, A. R., Daniel, J. S., and Portmann, R. W.: Nitrous oxide: The dominant ozone-depleting substance emitted in the 21st century, *Science*, 326, 123–125, doi: 10.1126/science.1176985, 2009.
- Rees, R. M., Augustin, J., Alberti, G., Ball, B. C., Boeckx, P., Cantarel, A., Castaldi, S., Chirinda, N., Chojnicki, B., Giebels, M., Gordon, H., Grosz, B., Horvath, L., Juszczak, R., Kasimir Klemetsson, Å., Klemetsson, L., Medinets, S., Machon, A., Mapanda, F., Nyamangara, J., Olesen, J. E., Reay, D. S., Sanchez, L., Sanz Cobena, A., Smith, K. A., Sowerby, A., Sommer, M., Soussana, J. F., Stenberg, M., Topp, C. F. E., van Cleemput, O., Vallejo, A., Watson, C. A., and Wuta, M.: Nitrous oxide emissions from European agriculture – an analysis of variability and drivers of emissions from field experiments, *Biogeosciences*, 10, 2671–2682, doi:10.5194/bg-10-2671-2013, 2013.
- Saikawa, E., Prinn, R. G., Dlugokencky, E., Ishijima, K., Dutton, G. S., Hall, B. D., Langenfelds, R., Tohjima, Y., Machida, T., Manizza, M., Rigby, M., O'Doherty, S., Patra, P. K., Harth, C. M., Weiss, R. F., Krummel, P. B., van der Schoot, M., Fraser, P. J., Steele, L. P., Aoki, S., Nakazawa, T., and Elkins, J. W.: Global and regional emissions estimates for N₂O, *Atmos. Chem. Phys.*, 14, 4617–4641, doi:10.5194/acp-14-4617-2014, 2014.
- Skamarock, W., Klemp, J., Dudhia, J., Gill, D., Barker, D., Duda, M., Huang, X., Wang, W., and Powers, J.: A description of the advanced research WRF version 3, NCAR/TN–475+STR, Natl. Cent. for Atmos. Res., Boulder, Colo, 2008.
- Tian, H., Xu, X., Liu, M., Ren, W., Zhang, C., Chen, G., and Lu, C.: Spatial and temporal patterns of CH₄ and N₂O fluxes in terrestrial ecosystems of North America during 1979–2008: Application of a global biogeochemistry model, *Biogeosciences*, 7, 2673–2694, doi:10.5194/bg-7-2673-2010, 2010.
- Turner, P. T., Griffis, T. J., Lee, X., Baker, J. M., Venterea, R. T., and Wood, J. D.: Indirect nitrous oxide emissions from streams within the US Corn Belt scale with stream order, *Proc Natl Acad Sci U S A.* 112(32), 9839–9843, doi:10.1073/pnas.1503598112, 2015.
- USDA National Agricultural Statistics Service. Statistics of fertilizer and pesticides. Available at https://www.nass.usda.gov/Publications/Ag_Statistics/2011/Chapter14.pdf, USDA-NASS, Washington, DC, 2011.
- Wagner-Riddle, C., Furon, A., McLaughlin, N. L., Lee, I., Barbeau, J., Jayasundara, S., Parkin, G., Von Bertoldi, P., and Warland, J.: Intensive measurement of nitrous oxide emissions from a corn-soybeanwheat rotation under two contrasting management systems over 5 years, *Global Change Biol.*, 13(8), 1722–1736, doi:10.1111/j.1365-2486.2007.01388.x, 2007.
- Xiang, B., Miller, S. M., Kort, E. A., Santoni, G. W., Daube, B. C., Commane, R., Angevine, W. M., Ryerson, T. B., Trainer, M.



K., Andrews, A. E., Nehrkorn, T., Tian, H., and Wofsy, S. C.: Nitrous oxide (N_2O) emissions from California based on 2010 CalNex airborne measurements, *J. Geophys. Res. Atmos.*, 118, 2809–2820, doi:10.1002/jgrd.50189, 2013.

Zhang, X., Lee, X., Griffis, T. J., Baker, J. M., and Xiao, W.: Estimating regional greenhouse gas fluxes: an uncertainty analysis of planetary boundary layer techniques and bottom-up inventories, *Atmos. Chem. Phys.*, 14, 10705-10719,

5 doi:10.5194/acp-14-10705-2014, 2014.



Table 1. WRF- Chem model configuration.

Basic equations	Non-hydro mode
Time-integration scheme	Runge-Kutta 3rd order
Time step for integration	120 s
Microphysics	WRF Single-Moment (WSM) 5-class scheme
Longwave radiation	Rapid Radiative Transfer Model (RRTM)
Shortwave radiation	Goddard Shortwave scheme
Cumulus	Grell-Devenyi ensemble scheme
Boundary-layer	Yonsei University Scheme (YSU) scheme
Surface-layer	Monin-Obukhov Similarity scheme
Land-surface	Community Land Model Version 4 (CLM4)

5

10

15

20

25

30

35

40

**Table 2.** Experimental and optimized flux multiplier M_F . Values in brackets are constrained agricultural emission flux in units of $\text{nmol m}^{-2} \text{s}^{-1}$.

Time	June 1 – 20	August 1 – 20	October 1 – 20	December 1 – 20
Experimental	0, 1, 25	0, 1, 12	0, 1, 3	0, 1, 6
Optimized ^a	19.0 (2.91)	9.3 (1.43)	3.4 (0.52)	3.0 (0.47)
Optimized ^b	22.5 (3.44)	11.6 (1.77)	3.8 (0.59)	3.6 (0.55)
Optimized ^c	28.1 (4.29)	13.0 (1.99)	4.7 (0.72)	4.3 (0.66)

Notes: a, b, c: using observation data at heights of 32, 100, and 185 m, respectively.

5

10

15

20

25

30

35

40



Table 3. Modeled and observed N₂O mixing ratio enhancements (ppb) for 1900 and 2000 UTC from NOAA. Measurements from Niwot Ridge (NWR) were used as background to determine the enhancement.

Site ID	Sample height (m)	Within modeling domain					Outside modeling domain		
		WBI	LEF	SCT	BAO	Mean	AMT	WKT	Mean
		378.9	396	304.8	300	ΔC	107	457.1	ΔC
June 1 – 20	Observation	3.28	0.80	0.79	0.22	1.27	0	0.46	0.23
	Model with $M_F = 1$	0.14	0.17	0.28	0.14	0.18	–	–	–
	Model with $M_F = 25$	3.67	1.26	0.90	0.20	1.51	–	–	–
August 1 – 20	Observation	0.69	-0.04	0.40	0.35	0.35	-0.77	0.02	0.02
	Model with $M_F = 1$	0.44	0.13	0.36	0.12	0.26	–	–	–
	Model with $M_F = 12$	2.82	0.87	0.41	0.15	1.06	–	–	–
October 1 – 20	Observation	-0.03	-0.55	0.50	0.11	0.01	-0.79	-0.35	-0.57
	Model with $M_F = 1$	0.86	0.56	0.58	0.21	0.55	–	–	–
	Model with $M_F = 3$	1.52	0.85	0.66	0.22	0.81	–	–	–
December 1 – 20	Observation	0.99	0.43	1.26	0.61	0.82	0.49	0.79	0.64
	Model with $M_F = 1$	1.22	0.36	0.85	0.14	0.64	–	–	–
	Model with $M_F = 6$	2.98	0.55	1.25	0.15	1.23	–	–	–

Notes: AMT – Argyle, Maine; BAO – Boulder Atmospheric Observatory, Colorado; LEF – Park Falls, Wisconsin; SCT – Beech Island, South Carolina; WBI – West Branch, Iowa; WKT – Moody, Texas.

5

10

15

20

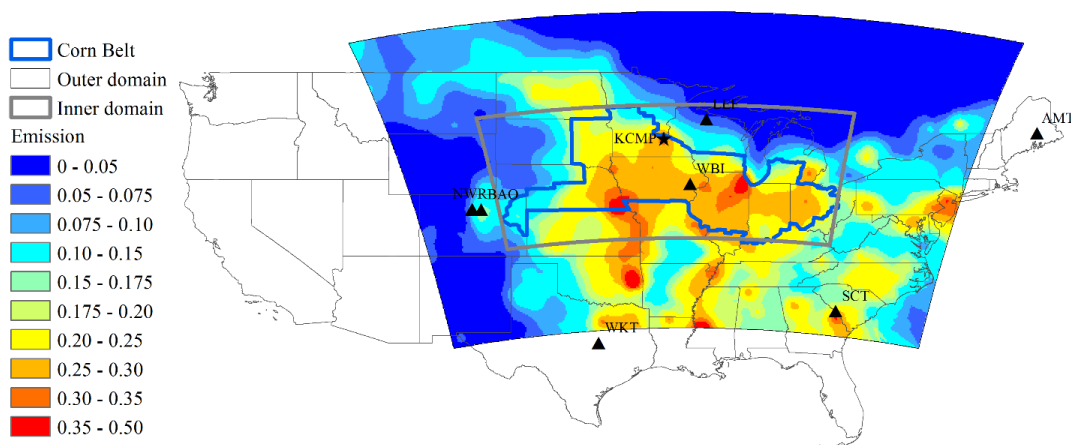


Figure 1. Locations of the N_2O monitoring sites, scope of the Corn Belt, modeling domains, and the default N_2O emission flux in $\text{nmol m}^{-2} \text{s}^{-1}$. KCMP – Minnesota; NWR – Niwot Ridge, Colorado; AMT – Argyle, Maine; BAO – Boulder Atmospheric Observatory, Colorado; LEF – Park Falls, Wisconsin; SCT – Beech Island, South Carolina; WBI – West Branch, Iowa; WKT – Moody, Texas.

5

10

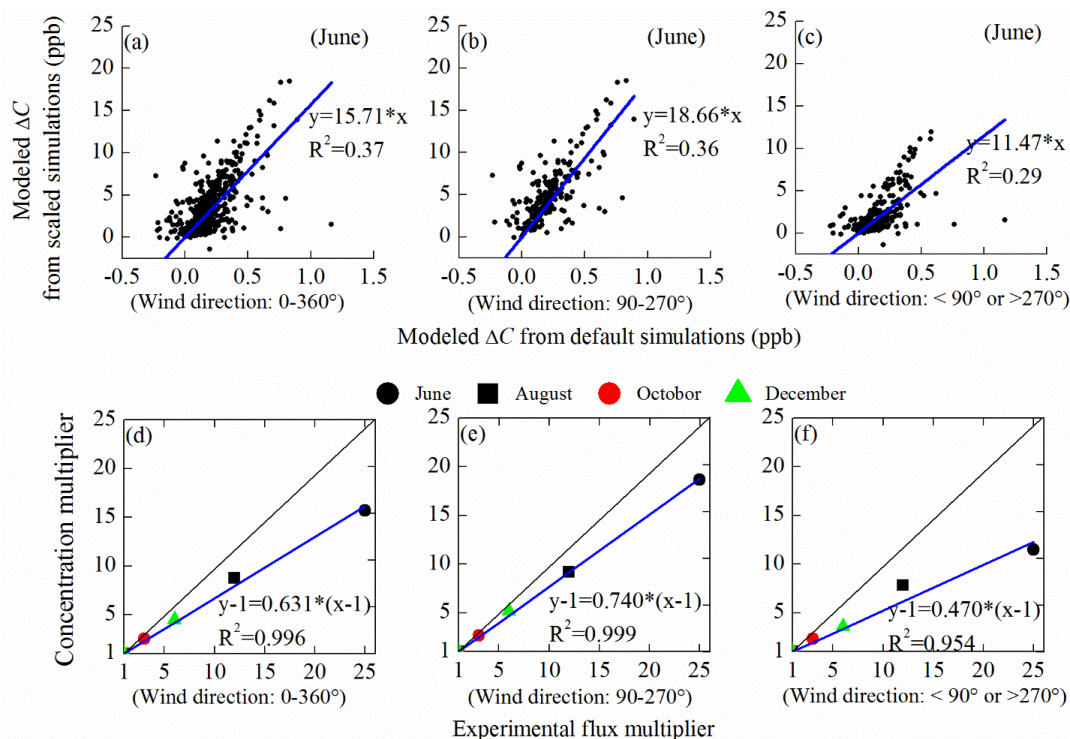


Figure 2. Relationships of for different model runs between concentration multiplier and experimental flux multiplier. The modeled N_2O mixing ratio enhancement ΔC was obtained from default and scaled simulations for 185 m at the KCMP tower. The regression slope in panels a – c is represented by the black circle in panels d – f.

5

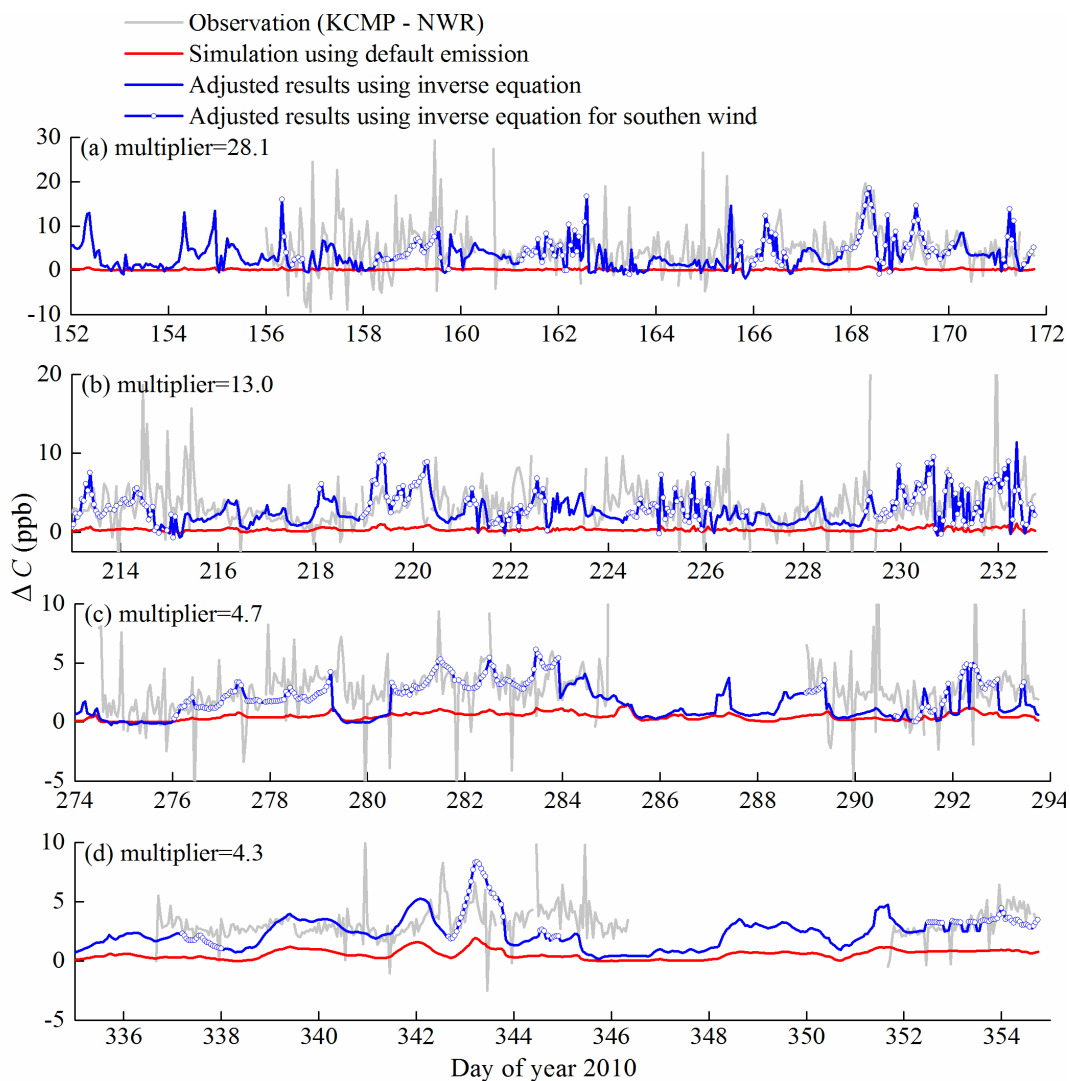


Figure 3. Comparison of N_2O mixing ratio enhancement (ΔC) between observation (grey line), default model simulation (red line), and the scaled model simulation (blue line) for the height of 185 m at the KCMP tower site. Periods with south wind (wind direction: $90 - 270^\circ$) are marked by dots.

5

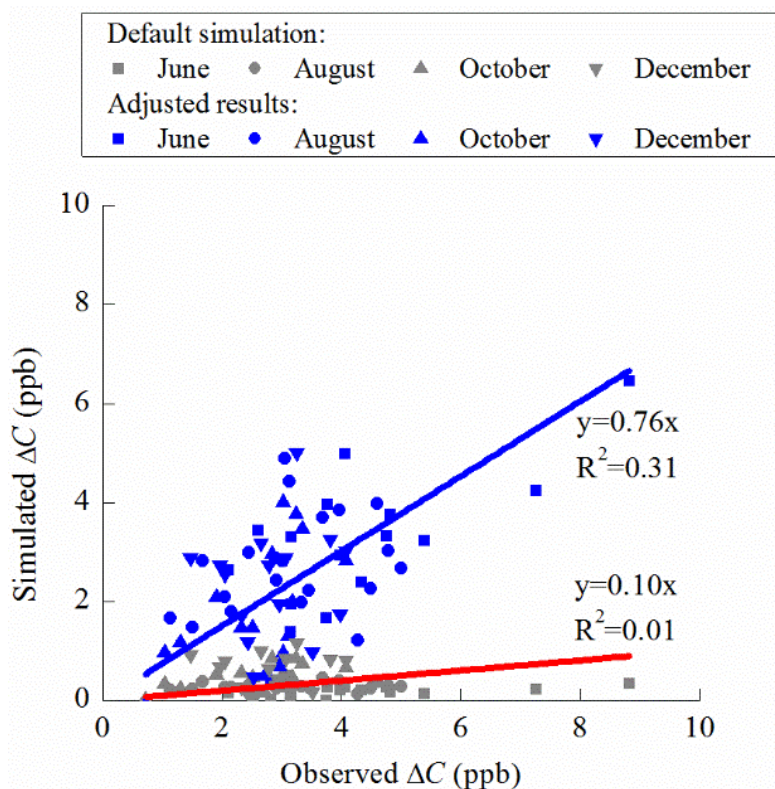


Figure 4. Correlations between the observed and scaled daily N_2O mixing ratio enhancement (ΔC) at the KCMP tower at 185 m.

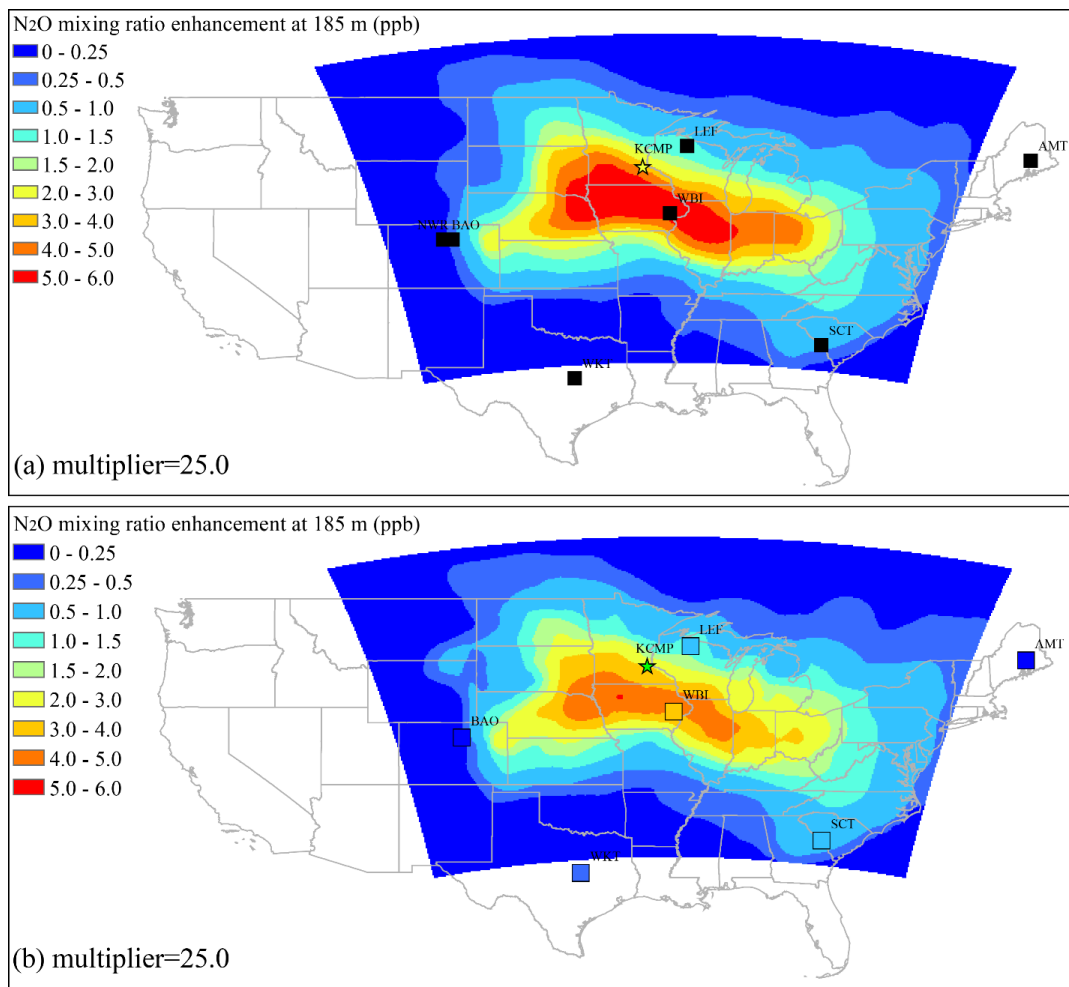


Figure 5. Spatial characteristics of the mean modeled N₂O mixing ratio enhancement during June 1 – 20: (a) modeled results for all hours; (b) modeled results for UTC hours 19 and 20 only.

5

10

15

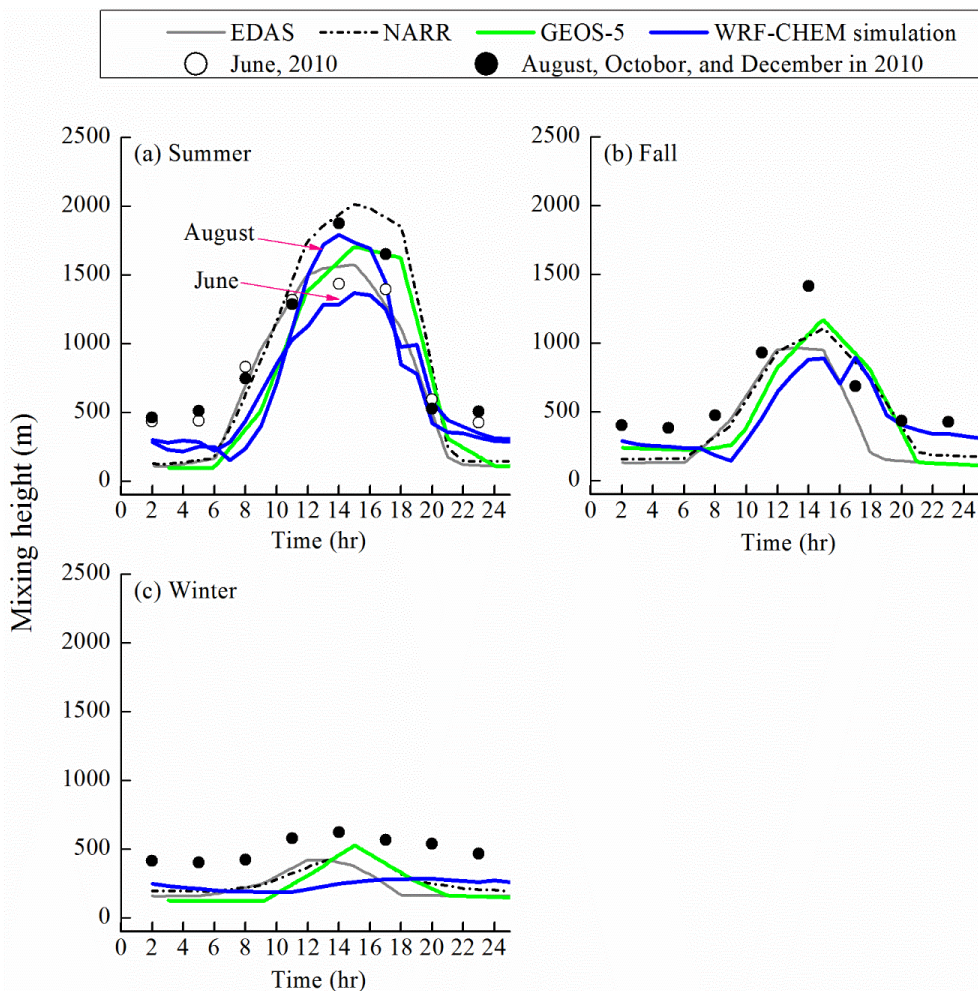


Figure 6. Simulated mixing height at the KCMP tower site in the present study (blue lines) and in Kim et al. (2013) (grey, black, and green lines) and the NCEP-NARR data (dots).